# Mechanical Tunability via Hydrogen Bonding in Metal–Organic Frameworks with the Perovskite Architecture

**ARTICLE** *in* JOURNAL OF THE AMERICAN CHEMICAL SOCIETY · MAY 2014

Impact Factor: 12.11 · DOI: 10.1021/ja500618z · Source: PubMed



**10 AUTHORS**, INCLUDING:

Zheshuai Lin
Chinese Academy of Sciences
**170** PUBLICATIONS **2,687** CITATIONS
SEE PROFILE

Sebastian Henke
Ruhr-Universität Bochum
**33** PUBLICATIONS **496** CITATIONS
SEE PROFILE

Michael Thomas Wharmby
Diamond Light Source
**18** PUBLICATIONS **435** CITATIONS
SEE PROFILE

Erica Bithell
University of Cambridge
**35** PUBLICATIONS **412** CITATIONS
SEE PROFILE

JACS
JOURNAL OF THE AMERICAN CHEMICAL SOCIETY
Communication
pubs.acs.org/JACS

# Mechanical Tunability via Hydrogen Bonding in Metal–Organic Frameworks with the Perovskite Architecture

Wei Li,[†] A. Thirumurugan,[‡] Phillip T. Barton,[§] Zheshuai Lin,*[,∥] Sebastian Henke,[†] Hamish H.-M. Yeung,[†,¶] Michael T. Wharmby,[†] Erica G. Bithell,[⊥] Christopher J. Howard,[#] and Anthony K. Cheetham*[,†]

[†]Department of Materials Science and Metallurgy, University of Cambridge, Cambridge CB3 0FS, U.K.

[‡]School of Chemistry, Indian Institute of Science Education and Research (IISER-TVM), Thiruvananthapuram, Kerala 695016, India

[§]Materials Research Laboratory (MRL) and Materials Department, University of California, Santa Barbara, California 93106, United States

[∥]Beijing Center of Crystal R&D, Technical Institute of Physics and Chemistry, Chinese Academy of Sciences, P.O. Box 2711, Beijing 100080, P. R. China

[⊥]Institute of Continuing Education, University of Cambridge, Madingley Hall, Madingley, Cambridge CB23 8AQ, U.K.

[¶]International Center for Young Scientists (ICYS), International Center for Materials Nanoarchitectonics (WPI-MANA), National Institute for Materials Science, Namiki 1-1, Tsukuba, Ibaraki 305-0044, Japan

[#]School of Engineering, University of Newcastle, Callaghan, New South Wales 2308, Australia

Supporting Information

**ABSTRACT:** Two analogous metal–organic frameworks (MOFs) with the perovskite architecture, $[C(NH_2)_3][Mn(HCOO)_3]$ (**1**) and $[(CH_2)_3NH_2][Mn(HCOO)_3]$ (**2**), exhibit significantly different mechanical properties. The marked difference is attributed to their distinct modes of hydrogen bonding between the A-site amine cation and the anionic framework. The stronger cross-linking hydrogen bonding in **1** gives rise to Young's moduli and hardnesses that are up to twice those in **2**, while the thermal expansion is substantially smaller. This study presents clear evidence that the mechanical properties of MOF materials can be substantially tuned via hydrogen-bonding interactions.

Perovskite $ABO_3$ materials have been studied intensively in physics, chemistry, and materials science because of their interesting and technologically important properties, including ferroelectricity, superconductivity, magnetoresistance, and catalysis.[1] The recent emergence of $ABX_3$-type metal–organic frameworks (MOFs) opens up a new hybrid route toward artificial perovskite structures, which significantly increases the diversity of this intriguing family of materials.[2] For example, Wang et al.[2a] reported a family of MOF perovskites, $[AmineH^+][M(HCOO)_3]$ ($AmineH^+$ = $[CH_3NH_3]^+$, $[CH_3CH_2NH_3]^+$, $[(CH_3)_2NH_2]^+$, $[(CH_2)_3NH_2]^+$, $[(NH_2)_3C]^+$; M = $Mn^{2+}$, $Co^{2+}$, $Ni^{2+}$, $Cu^{2+}$, $Zn^{2+}$), in which the A, B, and X sites are occupied by the amine cations, metal ions, and formate ligands, respectively. Like the classical perovskite oxides, these MOF perovskites exhibit many fascinating physical properties, such as ferroelectricity,[2e,f] ferroelasticity,[3] and multiferroicity.[4] Compared with the conventional oxides, MOF perovskites offer promising opportunities for tuning and modulation of material properties via diverse structural and chemical variability.[2a] More importantly, this new family of materials can exhibit additional functionalities and structural flexibility that cannot be achieved in perovskite oxides. We have shown that the ferroelectric and ferroelastic phase transitions in MOF perovskites are mainly triggered by the order–disorder of the A-site amine cations via hydrogen bonding rather than tilting of the B-site octahedra and/or A-site displacement as in their oxide counterparts.[2,3,4a,b] The recent report of the large lattice strain (~5%) through an orthorhombic to monoclinic transition in the ferroelastic MOF $[(CH_2)_3NH_2][Mn(HCOO)_3]$ further highlights the potential of these flexible MOF perovskites to undergo large structural changes in response to external stimuli.[3] Herein we analyze the impact of hydrogen bonding on the mechanical properties of two analogous MOF perovskites, $[C(NH_2)_3][Mn(HCOO)_3]$ (**1**) and $[(CH_2)_3NH_2][Mn(HCOO)_3]$ (**2**). The stronger cross-linking hydrogen bonding in **1** gives rise to Young's moduli and hardnesses that are up to twice those in **2**, while the thermal expansion is substantially smaller.

The frameworks in **1** and **2** are charge-balanced by guanidinium ($[(NH_2)_3C]^+$) and azetidium ($[(CH_2)_3NH_2]^+$), respectively, and crystallize in the orthorhombic system with similar cell parameters [*Pnna*, $a$ = 8.5211(3) Å, $b$ = 11.9779(4) Å, and $c$ = 9.0593(3) Å for **1**; *Pnma*, $a$ = 8.688(2) Å, $b$ = 12.303(3) Å, and $c$ = 8.875(2) Å for **2**].[2c,d] As shown in Figure 1, each $MnO_6$ octahedron within both frameworks is connected to six neighboring metal octahedra via anti–anti bridging $HCOO^-$ ligands, forming a three-dimensional $ReO_3$-type framework structure. The guanidinium or azetidium cations are situated in the centers of the $ReO_3$-type cavities, and both structures can be described as $ABX_3$-type perovskites in which A is the amine cation, B is the manganese ion, and the X is the formate ligand. In **1**, six bridging N–H···O hydrogen bonds from each guanidinium

**Received:** January 24, 2014
**Published:** May 9, 2014

   dx.doi.org/10.1021/ja500618z | J. Am. Chem. Soc. 2014, 136, 7801–7804

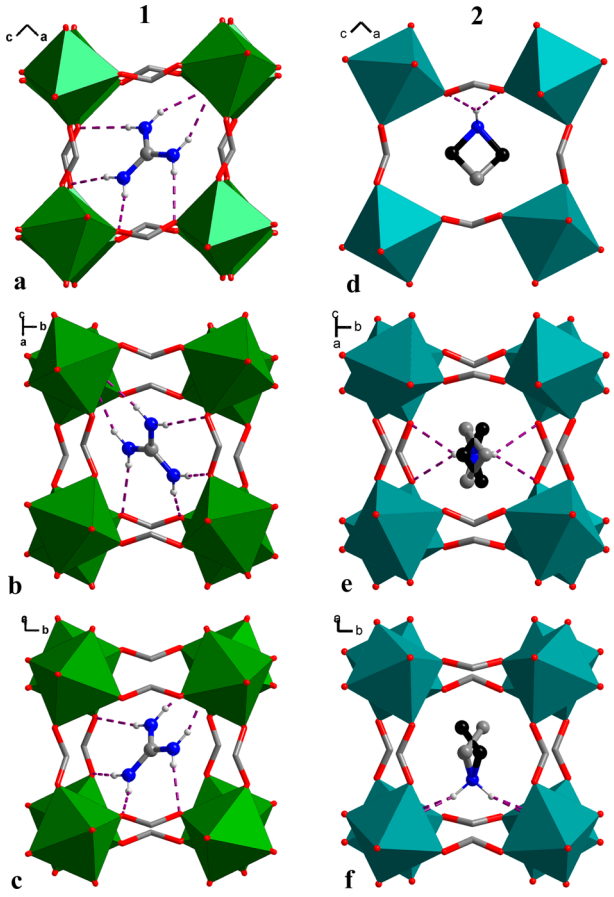


**Figure 1.** Framework structures of (a–c) $[C(NH_2)_3][Mn(HCOO)_3]$ (**1**) and (d–f) $[(CH_2)_3NH_2][Mn(HCOO)_3]$ (**2**) showing the pseudocubic perovskite unit cell: (a, d) (010); (b, e) (101); (c, f) $(10\bar{1})$. Color scheme: $Mn^{2+}$, green or teal; O, red; C, gray or black; N, blue. N–H···O bonds are represented as dashed purple lines. H atoms of formate ligands in **1** and **2** and $-CH_2-$ groups of the azetidium in **2** have been omitted for clarity. Note: the azetidium in **2** is equally disordered at two positions, as illustrated in gray and black colors.

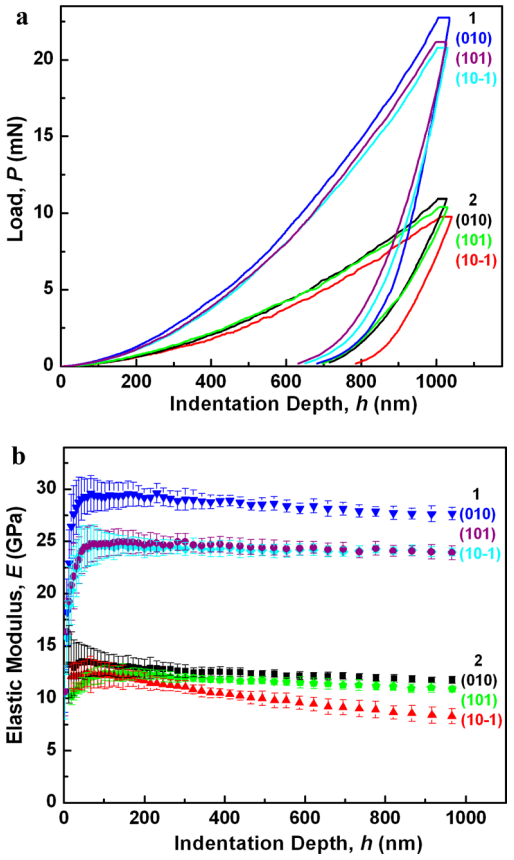


**Figure 2.** Nanoindentation data normal to the (010), (101), and $(10\bar{1})$ planes of single crystals of **1** and **2** measured with a Berkovich tip: (a) representative $P-h$ curves; (b) elastic moduli as a function of indentation depth. The error bars correspond to the standard deviations of 10–20 measurements that were made on each facet.

cation, with N···O distances of 2.953(2), 2.979(2), and 2.991(2) Å, are formed with the framework [Figure S1a in the Supporting Information (SI)].[2d] For **2**, each azetidium cation is hydrogen-bonded to the anionic framework by four N–H···O hydrogen bonds with N···O distances of 2.961(3) and 3.054(3) Å (Figure S1b).[2c] According to the Glazer notation for conventional $ABO_3$ perovskites, the octahedral tilting systems of **1** and **2** would be $a^-b^0a^-$ and $a^-b^+a^-$.[5]

Nanoindentation measurements were performed using a three-sided pyramidal Berkovich tip (end radius ~100 nm) in the continuous stiffness measurement (CSM) mode,[6,7] and the indenter axis was aligned normal to the (010), (101), and $(10\bar{1})$ planes of **1** and **2**. Representative load–penetration ($P-h$) curves obtained on all three facets of both frameworks are shown in Figure 2a. There are no discontinuity events during unloading and therefore no indications of any phase transitions. All of the $P-h$ plots exhibit large residual depths from unloading, indicating that a significant plastic deformation occurred underneath the Berkovich tip. The loading segments of the $P-h$ curves obtained on all three facets of **1** are smooth, while small discontinuities ("pop-ins") can be clearly observed for all facets of **2**.

These pop-ins, which indicate heterogeneous deformation, occur at several penetration depths ($h_{pop\text{-}in}$) with different magnitudes throughout the whole loading (Figure S2 and Table S1). It is evident that the values of $h_{pop\text{-}in}$ from all three facets of **2** are in multiples of ~6.2 Å and thus are integral multiples of the $d$ spacing of the pseudocubic unit cell [$d_{(101)}$ = 6.211(1) Å, $d_{(020)}$ = 6.152(2) Å, $d_{(10\bar{1})}$ = 6.211(1) Å]. Similar correlations between the pop-in magnitude and the underlying crystal length scale have been observed in studies of organic crystals.[8] The average values of the elastic moduli ($E$) and hardnesses ($H$) normal to the (010), (101), and $(10\bar{1})$ planes of **1** and **2** extracted from the $P-h$ curves are listed in Table 1. The elastic moduli of **1** and **2** lie between those of highly porous MOFs ($E \lesssim 9$ GPa, $\rho \approx 0.9–1.5$

**Table 1. Mechanical and DFT-Calculated Data for 1, 2, and $[(CH_3)_2NH_2][Mn(HCOO)_3]$ (3)[9]**

| MOF | H-bonding energy (eV)[a] | orientation | $E$ (GPa) | $H$ (GPa) |
|---|---|---|---|---|
| **1** | −4.63 | (010) | 28.6(4) | 1.25(4) |
| | | (101) | 24.5(5) | 1.18(4) |
| | | $(10\bar{1})$ | 23.5(6) | 1.11(5) |
| **2** | −3.01 | (010) | 12.6(3) | 0.66(3) |
| | | (101) | 11.7(3) | 0.59(3) |
| | | $(10\bar{1})$ | 11.5(4) | 0.58(3) |
| **3** | −3.38 | (012) | ~19[b] | ~0.8[b] |

[a]The hydrogen-bonding energy is referred to the calculated value of each pseudocubic unit cell. [b]Data were obtained from ref 9.


dx.doi.org/10.1021/ja500618z | J. Am. Chem. Soc. 2014, 136, 7801–7804

g/cm$^3$) and those of densely packed frameworks ($E \approx 20-100$ GPa, $\rho \gtrsim 2$ g/cm$^3$).[6] Moreover, they exhibit generally isotropic stiffness, which is different from many other MOF crystals.[6] It is noteworthy that the $E$ values of **1** are about twice those of **2** even though these MOFs have analogous framework structures. The elastic moduli of **1** and **2** are an order of magnitude lower than those of some well-known perovskite oxides,[10] for example, $BaTiO_3$[10a] ($E \approx 170$ GPa, tetragonal phase, $\rho \approx 6.02$ g/cm$^3$), $LaAlO_3$[10b] ($E \approx 300$ GPa, cubic phase, $\rho \approx 6.52$ g/cm$^3$), and $SrTiO_3$[10c] ($E \approx 280$ GPa, cubic phase, $\rho \approx 4.88$ g/cm$^3$). Additionally, the variation of the A-site metal in analogous perovskite oxides does not have such a significant effect on the elastic moduli as the hydrogen-bonding interactions between the A-site cation and the framework in MOF perovskites.[11] For example, the ∼22% radius difference of the A-site metals in orthorhombic $GdAlO_3$ and $ScAlO_3$ results in a variation of only ∼15% in the Young's modulus.[11c] The great compliance of **1** and **2**, in marked contrast to their oxide counterparts, is understandable in terms of the enhanced flexibility of the much larger and longer formate ligand in comparison to the $O^{2-}$ anion.[3]

The mechanical properties of **1** and **2** can be rationalized by examining the underlying crystal structures. Since **1** and **2** have similar anionic framework structures as well as a trivial density difference (**1** is only ∼3.3% denser than **2**),[2c,d] their contributions to the difference between the mechanical properties of **1** and **2** are expected to be minimal. Therefore, the substantial contrast between the mechanical properties of **1** and **2** can be attributed to the disparity in their hydrogen-bonding modes. As shown in Figures 1 and S1b, each azetidium in **2** is aligned within the *ac* plane and hydrogen-bonded to the two opposite edges within the same face of the pseudocubic unit cell by four N−H···O bonds. This adds only a few cross-linked constraints in one face of the pseudocubic unit cell normal to (101). However, each guanidinium in **1** is tilted by 48.7(5)° with respect to the *ac* plane and cross-links two perpendicular edges from two opposite faces of each pseudocubic unit cell. This total of six hydrogen bonds consequently gives more cross-linking constraints to the pseudocubic unit cell along all three orthogonal orientations. As a result of these greater constraints, the amine cation and anionic framework of **1** are bonded more tightly and resist larger mechanical deformation isotropically,[12] leading to a remarkably higher rigidity than for the less constrained structure of **2**.

The measured hardnesses of **1** are about twice those of **2**, revealing the strong structural dependence of framework plasticity (Table 1). Plastic deformation in nontwinned molecular crystals occurs via slip, which is facilitated by the dislocation movements under the influence of applied stress.[8b] High mobility of dislocations within the crystal generally results in more slipping. The larger amount of plastic deformation in **2** indicates that slip develops more easily, which is consistent with the periodic pop-ins observed from the loading segments of the indentation plots. The slip occurs due to the less cross-linked hydrogen bonding between the A-site azetidium and the anionic framework. Upon the accumulation of enough shear stress, slips develop intermittently in multiples of $d_{(101)}$, $d_{(020)}$, $d_{(10\bar{1})}$ (Figure S2.) High-pressure synchrotron single-crystal X-ray studies further support the above conclusion. Both **1** and **2** exhibit pressure-induced phase transitions: **1** transforms from orthorhombic to monoclinic between 1.28−1.68 GPa, while **2** shows a similar transition between only 0.41−0.66 GPa (Table S2).

The thermal expansion of **1** and **2** is also influenced by the different strengths of the hydrogen-bonding interactions in the two structures. As illustrated in Figure 3, the strongly hydrogen-bonded framework, **1**, exhibits significantly less strain compared

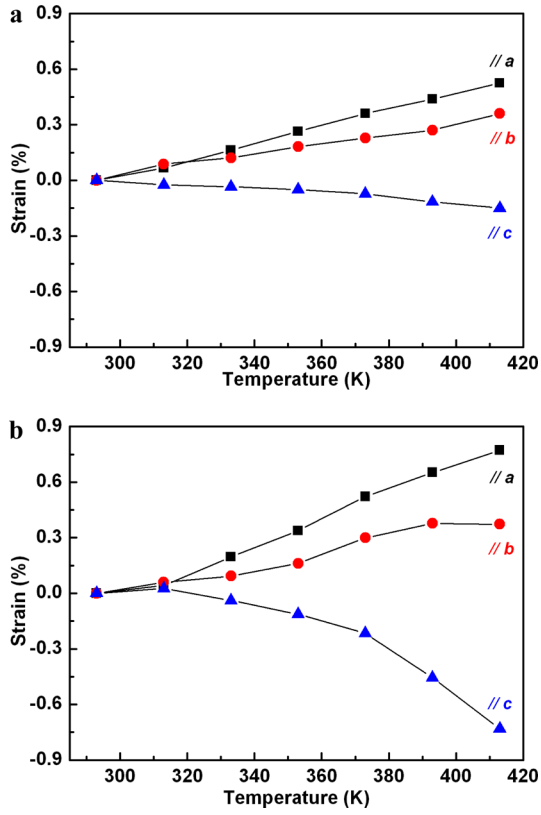


**Figure 3.** Thermal expansion measured for single crystals of (a) **1** and (b) **2**. The negative thermal expansion along *c* in both structures can be understood in terms of a classical strut and hinge mechanism for this structure type (see the SI for details). The linear thermal strains are referred to the three orthorhombic axes, and the lines drawn between data points are guides to the eye.

with the weakly hydrogen-bonded counterpart, **2**. Specifically, the thermal strains of the three orthogonal axes of **2** determined over the temperature range from 293 to 413 K are 1.5−4.9 times those of **1** (Table S3). Furthermore, the equivalent isotropic atomic displacement parameters ($U_{iso}$) for the manganese atom in **1** are about half those in **2** over the whole temperature range (Figure S4). This suggests that their average positions are more localized, perhaps as a result of the higher framework stiffness. This is a further indication of the effects of the different hydrogen-bonding arrangements in the two frameworks.[13]

In order to quantify the hydrogen-bonding energies in **1** and **2** and correlate them with their different mechanical properties, first-principles calculations were performed by the plane-wave pseudopotential method[14] based on density functional theory (DFT). The energy of hydrogen bonding between the A-site amine cations and the $[Mn(HCOO)_3]^-$ framework was obtained from the total energy of the whole structure by subtracting the contributions of the A-site amine cations and anionic frameworks. Our calculations revealed that the energies of hydrogen bonding are ca. −4.63 and −3.01 eV, respectively, per pseudocubic unit cell of **1** and **2** (ca. −0.77 and −0.75 eV per hydrogen bond, respectively), indicating a substantial energy difference in these two systems: the energy in **1** is about ∼55% greater than that in **2**. To further confirm the above results, the hydrogen-bonding energy of another analogous framework,


dx.doi.org/10.1021/ja500618z | J. Am. Chem. Soc. 2014, 136, 7801−7804

$[(CH_3)_2NH_2][Mn(HCOO)_3]$ (**3**) [$R\bar{3}c$, $a$ = 8.3211(3) Å and $c$ = 22.8856(12) Å], was also calculated.[9] The dimethylammonium ($[(CH_3)_2NH_2]^+$) in **3** is threefold-disordered and connected to the anionic framework by a three-dimensional arrangement of three hydrogen bonds in each pseudocubic unit cell (Figure S1c). Overall, the disordered cross-linked hydrogen bonding is expected to give intermediate energy and mechanical properties, and the hydrogen-bonding energy of ca. −3.38 eV per pseudocubic unit cell (ca. −0.84 eV per hydrogen bond) and the values $E \approx 19$ GPa and $H \approx 0.8$ GPa confirm this trend.[9]

In summary, the two MOF perovskites $[C(NH_2)_3][Mn(HCOO)_3]$ (**1**) and $[(CH_2)_3NH_2][Mn(HCOO)_3]$ (**2**) show significantly different mechanical properties as a result of their distinct modes of hydrogen bonding between the framework hosts and A-site amine cations. The stronger hydrogen bonding in **1** gives Young's moduli and hardnesses that are up to twice those in **2**, whereas the thermal expansion and atomic displacements are significantly smaller. This study presents clear evidence of the mechanical tunability of MOF materials, enabling scientists to control and direct the physical properties of MOFs via hydrogen-bonding and host−guest interactions.[15]

## ■ ASSOCIATED CONTENT

### Supporting Information

Experimental details and supporting cif files, figures, graphs, and tables. This material is available free of charge via the Internet at http://pubs.acs.org.

## ■ AUTHOR INFORMATION


### Corresponding Authors

akc30@cam.ac.uk
zslin@mail.ipc.ac.cn


### Notes

The authors declare no competing financial interest.

## ■ ACKNOWLEDGMENTS

W.L., S.H., H.H.-M.Y., M.T.W., and A.K.C. acknowledge the European Research Council for providing financial support. P.T.B. was supported by the National Science Foundation Graduate Research Fellowship Program. Z.L. acknowledges the support of the National Natural Science Foundation of China under Grants 11174297 and 91022036 and the National Basic Research Project of China (Grant 2011CB922204). S.H. is grateful to the Alexander von Humboldt Foundation for a postdoctoral fellowship. H.H.-M.Y. acknowledges support from the World Premier International Research Center Initiative on Materials Nanoarchitectonics (WPI-MANA) from MEXT, Japan. W.L. acknowledges Dr. Dave Allan and Dr. Mark Warren for assistance on beamline I19 at the Diamond Light Source (UK).

## ■ REFERENCES


(1) (a) Scott, J. F. *Ferroelectr. Rev.* **1998**, *1*, 1. (b) Bednorz, J. G.; Müller, K. A. *Rev. Mod. Phys.* **1998**, *60*, 585. (c) Zhang, X. X.; Hernandez, J. M. *Europhys. Lett.* **1999**, *47*, 487. (d) Suntivich, V.; May, K. J.; Gasteiger, H. A.; Goodenough, J. B.; Shao-Horn, Y. *Science* **2011**, *334*, 1183.

(2) (a) Wang, Z.; Hu, K.; Gao, S.; Kobayashi, H. *Adv. Mater.* **2010**, *22*, 1526. (b) Wang, X. Y.; Gan, L.; Zhang, S. W.; Gao, S. *Inorg. Chem.* **2004**, *43*, 4615. (c) Wang, Z. M.; Zhang, B.; Otsuka, T.; Inoue, K.; Kobayashi, H.; Kurmoo, M. *Dalton Trans.* **2004**, 2209. (d) Hu, K.-L.; Kurmoo, M.; Wang, Z.-M.; Gao, S. *Chem.—Eur. J.* **2009**, *15*, 12050. (e) Jain, P.; Dalal, N. S.; Toby, B. H.; Kroto, H. W.; Cheetham, A. K. *J. Am. Chem. Soc.* **2008**, *130*, 10450. (f) Jain, P.; Ramachandran, V.; Clark, R. J.; Zhou, H. D.; Toby, B. H.; Dalal, N. S.; Kroto, H. W.; Cheetham, A. K. *J. Am. Chem. Soc.* **2009**, *131*, 13625. (g) Pato-Doldán, B.; Sánchez-Andújar, M.; Gómez-Aguirre, L. C.; Yáñez-Vilar, S.; López-Beceiro, J.; Gracia-Fernández, C.; Haghighirad, A. A.; Ritter, F.; Castro-García, S.; Señarís-Rodríguez, M. A. *RSC Adv.* **2013**, *3*, 22404. (h) Shang, R.; Xu, G.-C.; Wang, Z.-M.; Gao, S. *Chem.—Eur. J.* **2014**, *20*, 1146. (i) Chen, S.; Shang, R.; Hu, K.-L.; Wang, Z.-M.; Gao, S. *Inorg. Chem. Front.* **2014**, *1*, 83.

(3) Li, W.; Zhang, Z.; Bithell, E. G.; Batsanov, A. S.; Barton, P. T.; Saines, P. J.; Jain, P.; Howard, C. J.; Carpenter, M. A.; Cheetham, A. K. *Acta Mater.* **2013**, *61*, 4928.

(4) (a) Fu, D.-W.; Zhang, W.; Cai, H.-L.; Zhang, Y.; Ge, J.-Z.; Xiong, R.-G.; Huang, S. D.; Nakamura, T. *Angew. Chem., Int. Ed.* **2011**, *50*, 11947. (b) Thomson, R. I.; Jain, P.; Cheetham, A. K.; Rawson, J. M.; Carpenter, M. A. *Phys. Rev. B* **2012**, *86*, No. 214304. (c) Stroppa, A.; Jain, P.; Marsman, M.; Perez-Mato, J. M.; Cheetham, A. K.; Kroto, H. W.; Picozzi, S. *Angew. Chem., Int. Ed.* **2011**, *50*, 5847. (d) Stroppa, A.; Barone, P.; Jain, P.; Perez-Mato, J. M.; Picozzi, S. *Adv. Mater.* **2013**, *25*, 2284. (e) Di Sante, D.; Stroppa, A.; Jain, P.; Picozzi, S. *J. Am. Chem. Soc.* **2013**, *135*, 18126.

(5) (a) Glazer, A. M. *Acta Crystallogr.* **1972**, *B28*, 3384. (b) Glazer, A. M. *Acta Crystallogr.* **1975**, *A31*, 756. (c) Stokes, H. T.; Hatch, D. M.; Campbell, B. J. *ISOTROPY*; Department of Physics and Astronomy, Brigham Young University: Provo, UT, 2007; stokes.byu.edu/isotropy.html.

(6) (a) Tan, J. C.; Merrill, C. A.; Orton, J. B.; Cheetham, A. K. *Acta Mater.* **2009**, *57*, 3481. (b) Tan, J.-C.; Cheetham, A. K. *Chem. Soc. Rev.* **2011**, *40*, 1059.

(7) (a) Varughese, S.; Kiran, M. S. R. N.; Ramamurty, U.; Desiraju, G. R. *Angew. Chem., Int. Ed.* **2013**, *52*, 2701. (b) Ramamurty, U.; Jang, J. *CrystEngComm* **2014**, *16*, 12.

(8) (a) Kiran, M. S. R. N.; Varughese, S.; Reddy, C. M.; Ramamurty, U.; Desiraju, G. R. *Cryst. Growth Des.* **2010**, *10*, 4650. (b) Varughese, S.; Kiran, M. S. R. N.; Solanko, K. A.; Bond, A. D.; Ramamurty, U.; Desiraju, G. R. *Chem. Sci.* **2011**, *2*, 2236. (c) Kiran, M. S. R. N.; Varughese, S.; Ramamurty, U.; Desiraju, G. R. *CrystEngComm* **2012**, *14*, 2489. (d) Varughese, S.; Kiran, M. S. R. N.; Ramamurty, U.; Desiraju, G. R. *Chem.—Asian J.* **2012**, *7*, 2118. (e) Krishna, G. R.; Kiran, M. S. R. N.; Fraser, C. L.; Ramamurty, U.; Reddy, C. M. *Adv. Funct. Mater.* **2013**, *23*, 1422.

(9) Tan, J.-C.; Jain, P.; Cheetham, A. K. *Dalton Trans.* **2012**, *41*, 3949.

(10) (a) Wang, J. J.; Meng, F. Y.; Ma, X. Q.; Xu, M. X.; Chen, L. Q. *J. Appl. Phys.* **2010**, *108*, No. 034107. (b) Carpenter, M. A.; Sinogeikin, S. V.; Bass, J. D.; Lakshtanov, D. L.; Jacobsen, S. D. *J. Phys.: Condens. Matter* **2010**, *22*, No. 035403. (c) Becke, R. O. *Phys. Rev. A* **1988**, *38*, 3098.

(11) (a) Bass, J. D. *Phys. Earth Planet. Inter.* **1984**, *36*, 145. (b) Huang, C. W.; Ren, W.; Nguyen, V. C.; Chen, Z.; Wang, J.; Sritharan, T.; Chen, L. *Adv. Mater.* **2012**, *24*, 4170. (c) Verma, A. S. *Solid State Commun.* **2013**, *158*, 34.

(12) Giddy, A. P.; Dove, M. T.; Pawley, G. S. *Acta Crystallogr.* **1993**, *A49*, 697.

(13) (a) Furman, J. D.; Burwood, R. P.; Tang, M.; Mikhailovsky, A. A.; Cheetham, A. K. *J. Mater. Chem.* **2011**, *21*, 6595. (b) George, N. C.; Pell, A. J.; Dantelle, G.; Page, K.; Llobet, A.; Balasubramanian, M.; Pintacuda, G.; Chmelka, B. F.; Seshadri, R. *Chem. Mater.* **2013**, *25*, 3979.

(14) Payne, M. C.; Teter, M. P.; Allan, D. C.; Arias, T. A.; Joannopoulos, J. D. *Rev. Mod. Phys.* **1992**, *64*, 1045.

(15) (a) Horike, S.; Shimomura, S.; Kitagawa, S. *Nat. Chem.* **2009**, *1*, 695. (b) Yu, J.; Cui, Y.; Wu, C.-D.; Yang, Y.; Wang, Z.; O'Keeffe, M.; Chen, B. *Angew. Chem., Int. Ed.* **2012**, *51*, 10542. (c) Sakata, Y.; Furukawa, S.; Kondo, M.; Hirai, K.; Horike, N.; Takashima, Y.; Uehara, H.; Louvain, N.; Meilikhov, M.; Tsuruoka, T.; Isoda, S.; Kosaka, W.; Sakata, O.; Kitagawa, S. *Science* **2013**, *339*, 193. (d) Grobler, I.; Smith, V. J.; Bhatt, B. M.; Herbert, S. A.; Barbour, L. J. *J. Am. Chem. Soc.* **2013**, *135*, 6411. (e) Talin, A. A.; Centrone, A.; Ford, A. C.; Foster, M. E.; Stavila, V.; Haney, P.; Kinney, R. A.; Szalai, V.; Gabaly, F. E.; Yoon, H. P.; Léonard, F.; Allendorf, M. D. *Science* **2014**, *343*, 66.

JACS
JOURNAL OF THE AMERICAN CHEMICAL SOCIETY
Spotlights
pubs.acs.org/JACS

# Spotlights on Recent *JACS* Publications

## BUBBLE, BUBBLE, TOIL AND TROUBLE, NANOCRYSTALS ON THE DOUBLE

Researchers use tiny crystalline materials called nanocrystals in applications that include electronics, solar energy, and medicine. These tiny tools can be created almost like a soup, with carefully mixed and heated ingredients swirling in a liquid. To get just the right shape and composition, researchers need to ensure that specific crystal faces grow while others stay dormant. While adding components to "seal off" certain faces has worked to a degree, the nanocrystal soups could be of higher quality if researchers had a better idea of exactly how each variable affects growth. Kevin Ryan and colleagues perform experiments to tease out the contributions from each variable (DOI: 10.1021/ja501591n).

The team focuses on a crystal that contains copper, tin, and selenium as it is an important photovoltaic material and also because this material can easily adopt two different crystalline structures. The results show that fine-tuning the selection of ingredients, how they are combined, and the reaction temperatures greatly affects the shape and structure of the resulting particles. Much like a master chef laying out a recipe for the perfect dish, the researchers create a set of best protocols to obtain each crystal phase and shape composition.
**Jenny Morber,** Ph.D.

## SMALL BONDS A BIG DEAL IN PEROVSKITE SOLAR CELLS

Inorganic−organic perovskites have attracted tremendous attention recently due to their interesting and technologically important properties, especially as new multiferroic and photovoltaic materials. Therefore, chemists have carefully studied these materials and learned that their properties are highly tunable, depending on their chemical composition and exact structure. A new type of perovskite material based on metal−organic frameworks (MOFs) has shown greater tunable properties than the more conventional metal oxides.

Now Zheshuai Lin, Anthony Cheetham, and co-workers probe the structures even further and find that two analogous MOF perovskites show markedly different properties, depending on how they hydrogen-bond (DOI: 10.1021/ja500618z). Both of the perovskites have similar $[Mn(HCOO)_3]^-$ framework structures and are charge-balanced by guanidinium ($[(NH_2)_3C]^+$) and azetidium ($[(CH_2)_3NH_2]^+$), respectively. The guanidinium compound (**1**) has six hydrogen bonds per amine cation, while the azetidium compound (**2**) has two. As a result, compound **1** is more rigidly constrained, and this material is about twice as stiff and hard as compound **2**. However, **1** has lower thermal expansion and atomic displacement than **2**.

This work shows how small structural details can significantly influence the mechanical properties of hybrid perovskites (including important photovoltaic perovskite halides), which can in turn help chemists to better design and direct the physical properties of these important materials.
**Leigh Krietsch Boerner,** Ph.D.

## BRINGING A NEW TWIST TO NANORIBBONS

While Moore's law, the gold standard that predicts the improvement of performance in microprocessors, is reaching its limit with current manufacturing technology, molecular electronics may provide the means for continued improvement. Nanoribbons, predicted to be compatible with a larger and more diverse number of electronic applications than graphene, are promising molecular building blocks to fabricate various nanoscale semiconductor devices.

Now, Shengxiong Xiao, Fay Ng, Michael L. Steigerwald, Colin Nuckolls, and co-workers develop a novel bottom-up synthetic approach to electron-deficient nanoribbons from perylenediimide (PDI), a five-ring polycyclic aromatic hydrocarbon derivative (DOI: 10.1021/ja503533y). Through careful design of precursors, the researchers are able to synthesize helical nanoribbons as PDI dimers, trimers, and tetramers in good yields with precise control.

Experimental and computational studies reveal the unique yet multifaceted attributes of these nanoribbons, including optical, electronic, and charge-transport properties. This work not only demonstrates a class of desirable nanomaterials for organic light-emitting diode and solar cell applications but also opens an avenue whereby a variety of graphene ribbons can be designed and developed.
**Xin Su,** Ph.D.

## TRANSITION METAL COMPLEXES FOR QUANTUM COMPUTING

Although the notion of quantum computation has existed for four decades, successful implementation remains in its preliminary stages. Quantum computers use quantum-mechanical phenomena to perform calculations, such as the simulation of quantum behavior in chemical systems and factoring large semiprime numbers. Quantum computers also possess many advantages over classical computers; for example, they can achieve certain types of computations orders of magnitude faster. While digital computers encode data into binary digits known as bits, quantum computers use quantum bits, or qubits, and chemists are stepping up to create molecular candidates to fill this role.

Researchers led by Stephen Hill and Danna Freedman looked to empirically derive design principles for electronic spin-based qubits. Their team has analyzed two series of simple transition metal complexes to develop a set of design principles that should help guide the future development of an electron spin-based molecular qubit (DOI: 10.1021/ja5037397). As a proof-of-concept, it is notable that one of the complexes exhibits slow decoherence, which minimizes the chance of information loss, and rare Rabi oscillations, a phenomenon that is essential for establishing the viability of a species as a qubit. The aggregate of this research demonstrates one of the complexes, $[Ru(C_2O_4)_3]^{3-}$, to be a molecular qubit candidate and presents a beginning to a set of design principles that will

**Published:** May 27, 2014




dx.doi.org/10.1021/ja505175h | *J. Am. Chem. Soc.* 2014, 136, 7783−7784

help guide the synthetic development of electron spin-based molecular qubits for applications in quantum computing.
**Christine Herman,** Ph.D.

## SOLAR CELL ABSORBS IN NEAR-IR, PUSHES THEORETICAL EFFICIENCY HIGHER

Perovskite solar cells are a promising type of photovoltaic cell—a device or material able to convert the energy of light into electricity—because they are inexpensive and easy to make and have a high conversion efficiency. Recent versions of these devices have conversion efficiencies of over 15% with high open-circuit voltages, a measure of the amount of power that is available from a solar cell. Theoretically, perovskite photovoltaic cells can have over 30% conversion efficiencies if they can utilize more of the electromagnetic spectrum, from the ultraviolet to the infrared. However, existing cells do not absorb well over 780 nm because they have larger band gaps, a property that correlates directly with electrical conductivity of a material.

To address this problem, Mercouri Kanatzidis and coworkers synthesize two perovskite solid solutions—methylammonium tin iodide and its lead analogue—that can efficiently absorb into the near-IR at 1050 nm (DOI: 10.1021/ja5033259). The researchers are able to achieve this result because the energy band gaps of mixed Pb/Sn compounds do not follow the expected linear trend. Instead, they have a narrower band gap of less than 1.3eV, which allows the low-energy absorption. The scientists study a series of the devices using different ratios of tin to lead and identify a perovskite material with the broadest light absorption, showing that near-IR absorption is possible and that higher efficiency solar cells could be achieved in the near future.
**Leigh Krietsch Boerner,** Ph.D.